Journal of proteome research

Article

pubs.acs.org/jpr

Lipidomic Perturbations in Lung, Kidney, and Liver Tissues of p53 Knockout Mice Analyzed by Nanoflow UPLC-ESI-MS/MS

Se Mi Park,[†] Seul Kee Byeon,[†] Hyerim Sung,[‡,§] Soo Young Cho,[‡,§] Je Kyung Seong,[*,‡,§] and Myeong Hee Moon[*,†]

[†]Department of Chemistry, Yonsei University, Seoul 03722, Korea

[‡]College of Veterinary Medicine, BK21 Program for Veterinary Science and Research Institute of Veterinary Science, Seoul National University, Seoul 08826, Korea

[§]Korea Mouse Phenotyping Center (KMPC), Seoul 08826, Korea

Supporting Information

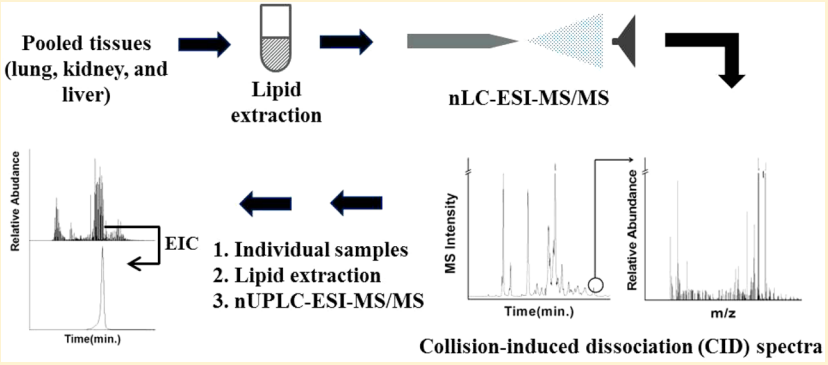

ABSTRACT: Lipids are important signaling molecules regulating biological processes under normal and diseased conditions. Although p53 mutation is well-known for causing cancer, the relationship between p53-related tumorigenesis and altered lipid profile is unclear. We profiled differences in lipid expressions in liver, lung, and kidney in p53 knockout (KO) mice by high-speed quantitative analysis of 320 lipids (399 species identified) using nanoflow ultrahigh performance liquid chromatography−tandem mass spectrometry (nUPLC-MS/MS). Lung tissues were most severely affected by the lack of p53 gene, as shown by significant reduction (24−44%, $P < 0.05$) in total phosphatidylcholine (PC), phosphatidylethanolamine (PE), sphingomyelin (SM), diacylglycerol (DG), and triacylglycerol (TG), and significant increases (30−50%) in phosphatidylserine (PS), phosphatidylinositol (PI), and monohexosylceramide (MHC). MHC levels increased in all tissues. Dihexosylceramide (DHC) level decreased only in kidney tissue. Most PI, PS, and phosphatidic acid (PA) species showing significant increases contained a saturated acyl chain (18:0) in lung and liver tissues. Neutral glycerolipids (16:0/22:0-DG and most TGs with saturated and monounsaturated acyl chains) decreased 2−4-fold in the liver tissue. Our results suggest that the lack of p53 and altered lipid profiles are closely related, but as their changes vary from one tissue to another, the lipid alterations are tissue-specific.

KEYWORDS: *lipidomic analysis, p53 knockout mouse, liver, kidney, lung, nUPLC-ESI-MS/MS*

INTRODUCTION

Cancer is currently a major global health concern despite significant developments made in the last few decades to improve health conditions. Lung and bronchial cancers were the most prevalent forms of cancer in both males and females, followed by prostate cancer in males and breast cancer in females, according to the United States National Center for Health Statistics (NCHS) in 2011.[1] p53 mutation is the most commonly reported mutation in various types of cancer.[2] The tumor suppressor gene encoding p53 protein has been extensively investigated by researchers around the world since it is known to prevent development of tumors by regulating cell-cycle, DNA recombination, gene amplification, and, most notably, apoptosis.[3] In response to various stress signals such as DNA damage along with hypoxia, telomere erosion, and microtubule inhibition, the amount of p53 protein increases significantly and inhibits cancer development.[4] Although p53-related studies have been extensively performed at the gene and protein levels, based on missense mutation, manipulation of mRNA by aromatase, or structural identification of p53-interacting protein called MDM2,[5−8] the influence of p53 mutation on lipids and lipid profiles has not been investigated. Studies have shown that p53 mutation alters lipid metabolism, resulting in lipid accumulation in mouse embryonic fibroblast and liver.[5] p53 mutation also causes lipid metabolism to shift to shorter fatty acyl chains of phosphatidylinositol (PI) in

Received: June 21, 2016
Published: September 1, 2016

DOI: 10.1021/acs.jproteome.6b00566
J. Proteome Res. 2016, 15, 3763−3772

mouse-derived pancreatic cancer cell lines, determined using mass spectrometry (MS).[9] The increase in phosphatidylcholine (PC) and total choline levels in human colon carcinoma cell lines witha disrupted p53 gene was determined using nuclear magneticmagnetic resonance (NMR) spectroscopy.[10]

Lipids play key roles in multiple cellular functions, including energy storage, cell signaling, and structural support.[11,12] Lipids are classified into various types such as phospholipids (PLs), glycerolipids (GLs), sphingolipids (SLs), sterol lipids, etc. Differences in head groups, length of fatty acyl chains, and degree of unsaturation give rise to a variety of lipid types. Each lipid class is further categorized into different subclasses based on their head groups, and their metabolism is significantly altered during development and progression of diseases. Rapid technical advances in MS have facilitated the determination of lipid molecular structures along with quantitative evaluation of diverse lipids at the molecular level. Combining the techniques of liquid chromatography (LC) with MS via electrospray ionization (ESI) has expanded the range of analytical performance in identifying as many lipids as possible, owing to the decrease in ionization suppression from the highly abundant species.[13−15] Recently, lipidomic analysis with LC-MS has been attempted to investigate lipid profiles in patient plasma or urine samples in various diseases, such as colorectal cancer,[16] breast cancer,[17,18] diabetes,[19] prostate cancer,[20,21] and Gaucher's disease.[22] Specifically, the use of nanoflow LC using capillary columns, prior to MS, is effective in acquiring an enhanced resolution of separation and also improves the sensitivity of detection at low levels (up to femtomolar levels) of lipid species,[23,24] owing to the reduced consumption of LC solvents. Lipids have been recognized as important signaling molecules that regulate biological processes not only in normal but also in diseased conditions.[25] Distinctly altered lipid profiles have been reported in cancer tissues of prostate, breast, and lymphomas.[26,27] However, relatively few studies have investigated global lipid changes under p53 deficiency.

In this study, the quantitative changes in lipid profiles of lung, kidney, and liver tissues of mice under the deficiency of p53 gene (hereafter referred to p53 knockout or p53 KO) were investigated using nanoflow LC-tandem mass spectrometry (nLC-ESI-MS/MS) to evaluate the effects of p53 deficiency on various PLs, GLs, and SLs. We compared the lipid profiles of the lung, kidney, and liver tissues between wild type (WT) and p53 KO mice. For the nontargeted lipid identification of each tissue type, a pooled tissue sample of each organ was analyzed using nLC-ESI-MS/MS. Based on the lipid species identified from each pooled sample, high-speed targeted-quantitation was accomplished for each individual sample using nanoflow ultrahigh performance LC-MS/MS (nUPLC-ESI-MS/MS) with the selected reaction monitoring (SRM) method. To the best of our knowledge, this is the first study to assess the similarities and differences in lipid profiles, among three different tissue types in p53 KO mice, using statistical analyses.

EXPERIMENTAL PROCEDURES

Materials and Reagents

For optimization of nLC-ESI-MS/MS run conditions, 37 lipid standards were used in this study. They are 12:0-lysophosphatidylcholine (LPC), 18:1-LPC, 14:0-lysophosphatidylethanolamine (LPE), 12:0/12:0-phosphatidylcholine (PC), 13:0/13:0-PC, 14:0/16:0-PC, 16:0/14:0-PC, 16:0/16:0-PC, 18:1/18:0-PC, 20:0/20:0-PC, 12:0/12:0-phosphatidylethanolamine (PE), 14:0/14:0-PE, 18:0/22:6-PE, 12:0-lysophosphatidic acid (LPA), 18:0-LPA, 12:0-lysophosphatidylglycerol (LPG), 14:0-LPG, 14:0/14:0-phosphatidic acid (PA), 12:0/12:0-phosphatidylglycerol (PG), 15:0/15:0-PG, 16:0/16:0-PG, 16:0/18:2-phosphatidylinositol (PI), 16:0/16:0-phosphatidylserine (PS), $(18:1)_4$-cardiolipin (CL), d18:0/12:0-sphingomyelin (SM), d18:1/16:0-SM, d18:1/18:0-SM, d18:1/24:0-SM, d18:1/12:0-glucosylceramide (GluCer), d18:1/18:0-GluCer, d18:1/16:0-lactosylceramide (LacCer), d18:1/16:0-galactosylceramide (GalCer), d18:1/14:0-Cer, d18:1/22:0-Cer, 16:0/18:1-diacylglycerol (DG), 18:1/18:1-DG, and 44:1(14:0/16:1/14:0)-triacylglycerol (TG). The lipid standards were purchased from Avanti Polar Lipids, Inc. (Alabaster, AL) and Matreya, LLC. (Pleasant Gap, PA). Absolute quantitation of lipids cannot be carried out as lipids with different head groups and acyl chains have different responses in MS. For the purpose of relative quantitation, 13:0/13:0-PC and 15:0/15:0-PG were used as internal standards (IS) in positive and negative ion mode, respectively, to compensate the fluctuation in MS responses throughout the run. HPLC grade methanol, acetonitrile, and isopropanol used for HPLC mobile phases were purchased from Avantor Performance Materials, Inc. (Center Valley, PA, USA). Methyl-*tert*-butyl ether (MTBE), NH_4HCO_2, NH_4OH, hematoxylin, and eosin were purchased from Sigma-Aldrich Co. LLC. (St. Louis, MO). Paraformaldehyde was purchased from Biosesang (Seongnam, Korea). Fused silica capillary tubes of 75 and 100 μm I.D. (360 μm O.D.) were purchased from Polymicro Technology, LLC (Phoenix, AZ). Watchers ODS-P C-18 particles (3 μm and 100 Å) were purchased from Isu Industry Corp. (Seoul, Korea) and 1.7 μm ethylene bridged hybrid (BEH) particles unpacked from XBridge BEH C18 column (1.7 μm, 2.1 mm × 100 mm), obtained from Waters (Milford, MA), were utilized for packing capillary LC columns.

Animals

Five-month-old male p53 KO mice and C57BL6/N mice (as control) were used. p53 KO mice were purchased from the Jackson Laboratory (Bar Harbor, ME) and were maintained in the animal facility at Seoul National University. The animals were housed at 24 ± 2 °C with a 12-h light/dark cycle and fed with a normal diet, NIH-31 from Zeigler Bros, Inc. (Gardners, PA) *ad libitum* with tap water. Animals were sacrificed by CO_2 exposure. This experimental protocol was carried out according to the "Guide for Animal Experiments" edited by Korean Academy of Medical Sciences and was approved by the Institutional Animal Care and Use Committee (IACUC) of Seoul National University.

Histological Analysis

Each organ was removed after euthanasia and fixed with 4% paraformaldehyde overnight at room temperature. The fixed tissue samples were dehydrated, cleared, and embedded in paraffin. A 4-μm section was taken from each of the embedded tissue pieces and stained with hematoxylin and eosin. The tissue sections were examined using a microscope equipped with a DP71 digital camera from Olympus Co. (Tokyo, Japan). Four to five images were captured from multiple stained pieces of adipose tissue from each mouse.

Lipid Extraction from Tissue Samples

A total of 36 tissue samples (lung, kidney, and liver from p53 KO mice (n = 6) and WT mice (n = 6) were provided in dried condition from the Korea Mouse Phenotyping Center.

DOI: 10.1021/acs.jproteome.6b00566
J. Proteome Res. 2016, 15, 3763−3772

Table 1. Identified/Quantified Numbers of Lipids in Each Category from Three Tissue Samples (lung, kidney, and liver) from p53 KO Mice Analyzed by nLC-ESI-MS/MS and Types of Precursor Ion and SRM Quantifier Ion for Each Lipid Class

	Identified/ quantified	Precursor → quantifier ion
PC	61/43	$[M + H]^+ \rightarrow [PCho + H]+$
PE	33/24	$[M + H]^+ \rightarrow [M + H - 141]^+$
DG	25	$[M + H]^+ \rightarrow [M + NH_4]^+ \rightarrow [M - RCOO]^+$
TG	100/48	$[M + H]^+ \rightarrow [M + NH_4]^+ \rightarrow [M - RCOO]^+$
SM	12	$[M + H]^+ \rightarrow [PCho + H]^+$
Cer	7	$[M + H]^+ \rightarrow [d18:1]^+$
MHC	3	$[M + H]^+ \rightarrow [d18:1]^+$
DHC	3	$[M + H]^+ \rightarrow [d18:1]^+$
PI	47	$[M - H]^- \rightarrow [RCOO]^-$
PG	38	$[M - H]^- \rightarrow [RCOO]^-$
PA	25	$[M - H]^- \rightarrow [RCOO]^-$
PS	45	$[M - H]^- \rightarrow [RCOO]^-$
total	399/320	

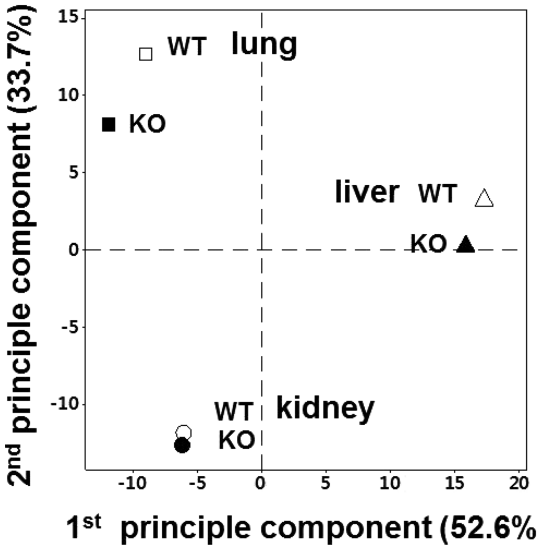

Figure 1. PCA plot of lung, kidney, and liver tissues showing the differences between WT (marked with open symbols) and p53 KO (marked with filled symbols) mice based on 320 quantified lipids.

Each tissue sample was crushed into a powder to make homogeneous mixtures, and small aliquots of each powder sample were taken for extraction. For nontargeted search of lipids from each organ, 1 mg of each individual animal sample was taken to make 6 mg of pooled sample. For lipid extraction, Folch method modified with MTBE/CH_3OH[28] was utilized. The pooled tissue powder (6 mg) was dissolved in 300 μL of CH_3OH and cooled in an ice bath for 10 min. Then 1000 μL of MTBE was added to the sample mixture and vortexed for an hour. For the phase separation, 250 μL of MS-grade H_2O was added and vortexed for 10 min at room temperature and centrifuged at 1000 × *g* for 10 min. The upper organic layer was transferred to a new tube. Then 300 μL of CH_3OH was added to the remaining lower aqueous layer, followed by sonication for 2 min and centrifugation for 10 min at 1000 × *g*. The upper organic layer was pipetted and added to the previously collected organic layer. This tube was wrapped with 0.45 μm MillWrap PTFE membrane from Millipore (Bedford, MA) during half day of lyophilization. This procedure keeps lipids from evaporating during freeze-drying process. Dried lipids were weighed and then reconstituted in $CHCl_3$:CH_3OH (3:7, v/v) to be stored at −30 °C. Prior to nLC-ESI-MS/MS analysis, this mixture was diluted with CH_3OH:H_2O (9:1, v/v) at a concentration of 5 μg/μL. For the targeted quantitation, 10 mg of each powdered tissue sample from each animal was taken for lipid extraction following the same procedures as described above.

Lipid Analysis Using nLC-ESI-MS/MS

Nontargeted qualitative analysis of lipids was accomplished with pooled tissue samples by using nLC-ESI-MS/MS, a model 1200 capillary LC pump system including an autosampler from Agilent Technologies (Santa Clara, CA) coupled with a model LTQ Velos ion trap mass spectrometer from Thermo Scientific (San Jose, CA). The analytical column was prepared in laboratory by packing Watchers ODS-P C18 resins (3 μm-100 Å) in a pulled tip silica capillary tube (75 μm I.D. and 360 μm O.D.) and the column length was adjusted to 7 cm. The capillary column was connected with a capillary tube from LC pump via a PEEK microcross from IDEX (Oak Harbor, WA) in which the other two ports were connected with a Pt wire for electric source and a pressure tube (20 μm I.D. capillary) to split the flow. The pressure tube was connected with an on/off valve so that flow from the pump can be blocked or split. The mobile

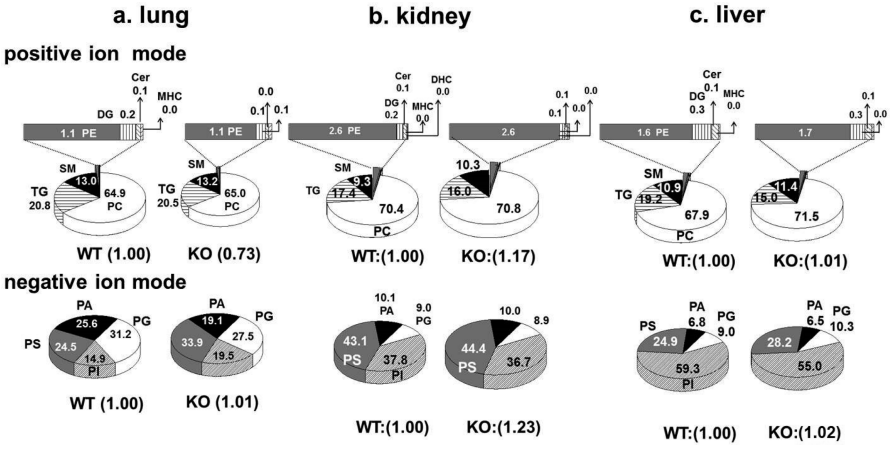

Figure 2. Relative abundance of each lipid category based on total peak area from (A) lung, (B) kidney, and (C) liver tissues of WT and p53 KO mice. Numbers in parentheses next to WT and KO represent the normalized value compared to WT.

DOI: 10.1021/acs.jproteome.6b00566
J. Proteome Res. 2016, 15, 3763−3772

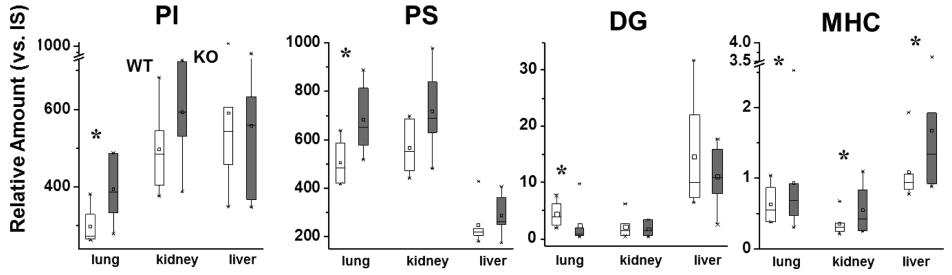

Figure 3. Relative amount (vs IS) of PI, PS, DG, and MHC in liver, kidney, and lung tissues between WT and p53 KO mice. Lipid category marked with asterisk (*) shows a significant change (>30%, $P < 0.05$) between WT and KO.

phases were H_2O:ACN (9:1, v/v) for A and IPA:CH_3OH:ACN (6:2:2, v/v/v)) for B, and both were added with a mixed modifier (5 mM HCO_2NH_4 and 0.05% NH_4OH) which was used in both positive and negative ion modes. During sample loading, 100% mobile phase A was used to deliver lipid sample to the analytical column at a flow rate of 600 nL/min for 10 min, with the valve off. Then, the mobile phase B was ramped to 40% over 1 min with the pump flow rate of 10 μL/min and the split flow valve on the so that the flow rate of the effluent from analytical column can be adjusted at 300 nL/min. The use of high pump flow with flow splitting was used to reduce dwell time. The mobile phase B was continuously ramped to 80% over 10 min, then to 100% over 20 min, and maintained at 100% for 29 min. After washing column, the mobile phase B was resumed at 0% over 1 min and then re-equilibrated for 18 min. The same gradient run condition was applied for both positive and negative ion mode of MS detection. The MS range for precursor scan was 250 to 1000 amu and 40% of normalized collision energy was applied for MS^2 analysis. The ESI voltage was 3 kV at both positive and negative ion modes. Determination of molecular structure of lipids was done by Li Pilot, a computer-based algorithm designed to determine lipid structure from the collision-induced dissociation (CID) spectra.[29]

For targeted quantitative analysis of identified lipids, nUPLC-ESI-MS/MS, a model nanoACQUITY UPLC from Waters coupled with a TSQ Vantage triple stage quadrupole MS from Thermo Scientific, was utilized with a similarly packed analytical column (100 μm I.D. and 360 μm O.D.) as used in the nontargeted profiling: the first 5 mm of the sharp needle tip was packed with 3 μm C-18 particles from Isu Industry Corp. while the remaining 6.5 cm of the column was packed with 1.7 μm BEH-particles from Waters. The flow rate for nUPLC-ESI-MS/MS was adjusted at 300 nL/min with the same mobile phase solutions. Sample loading (10 μg of lipid extracts containing two internal standards: 13:0/13:0-PC and 15:0/15:0-PG) was made at 1 μL/min for 10 min. Quantitation was done with selected reaction monitoring (SRM) method under a gradient condition modified to achieve a high speed separation: Mobile phase B ramped from 0% to 50% for 0.1 min, linearly increased to 80% for 2 min, and then to 100% for 6 min. It was maintained at 100% B for 14 min for compete elution and column washing. Then it was resumed to 0% B for 1 min and re-equilibrated for 4 min before the next run. For quantitation, ion detection was made in positive and negative ion modes alternatively with the scan width at m/z 2, scan time at 0.01 s, and ESI voltage at 3 kV. Lipid categories detected in positive ion mode were PCs, PEs, DGs, TGs, SMs, and Cers. PIs, PGs, PAs, and PSs were detected in negative ion mode. Collision energies were varied depending on the lipid types: 40 V for PCs, SMs, DGs, and TGs, 20 V for PEs, 30 V for Cer, monohexosylceramide (MHC), and DHC, and 35 V for PIs, and PGs. The linearity and robustness of the method has been validated in the previous papers, including the detection limit of low fmol using various classes of lipid standards.[30,31] Statistical analyses of data were performed with Mann−Whitney U-test using SPSS software (version 20.0, IBM Corp., Armonk, NY, USA), false discovery rate (FDR) using R (http://www.r-project.org), and principal component analysis (PCA) using Minitab 17 statistical software (http://www.minitab.co.kr).

RESULTS AND DISCUSSION

Nontargeted Analysis of Lipids Using nLC-ESI-MS/MS

For the nontargeted lipid profiling of mouse tissue sample (lung, kidney, and liver), pooled samples from each type of tissue were analyzed by nLC-ESI-MS/MS and molecular structures of individual lipid species were determined by data-dependent CID experiments. A total of 399 lipid species with molecular structures were identified—61 PCs, 33 PEs, 25 DGs, 100 TGs, 12 SMs, 7 Cers, 3 MHCs, 3 DHCs, 47 PIs, 38 PGs, 25 PAs, and 45 PSs—which were grouped under each tissue type based on slight variations: 387 for lung, 387 for kidney, and 362 for liver listed in Table S1 of the Supporting Information. While most species were identified by MS/MS (or MS^2) experiments, a few lipid classes, such as SMs, Cers, MHCs, and DHCs, were characterized by MS^3 in the negative ion mode.

Targeted Analysis of Lipids Using nUPLC-ESI-MS/MS

For the quantitative analysis of identified lipid molecules, samples from individual animals were analyzed by nUPLC with triple quadrupole MS using the SRM method. For high-throughput quantitation, an SRM time-table was applied for the rapid detection of 320 lipids in 20 min of separation time interval, programmed such that each individual lipid molecule was scanned during 2 min time intervals (±1 min of retention time). Since the average bottom width of a lipid peak during nUPLC separation was less than 1 min, it was enough to accommodate all species for quantitation. While PC and PE were identified based on their acyl chain compositions as well as regioisomers using qualitative analysis, they were quantified based on the total numbers of carbon atoms and double bonds in the acyl chain, since the dominant product ions of PCs and PEs in SRM quantitation were $[PCho + H]^+$ (m/z 184) and $[M + H - 141]^+$, respectively. TGs were also quantified without differentiating structural isomers. Therefore, the quantified numbers of PC, PE, and TG were reduced to 43, 24, and 48, respectively; lipids from all other classes were quantified based on their acyl chain structures. These quantified values are listed in Table 1 along with the type of precursor and quantifier ions for SRM quantitation. Results for the quantitative analysis of

DOI: 10.1021/acs.jproteome.6b00566
J. Proteome Res. 2016, 15, 3763−3772

Table 2. Relative Ratio (KO/WT) of Each Lipid Class Based on Total Peak Area (vs IS)[a]

Class	Lung			Kidney			Liver		
	WT	KO	KO/WT	WT	KO	KO/WT	WT	KO	KO/WT
PC	1569.01 ± 274.64	1148.82 ± 100.17	0.73 ± 0.14	969.04 ± 155.04	1134.76 ± 167.68	1.17 ± 0.26	2927.84 ± 412.08	3123.39 ± 485.02	1.07 ± 0.22
PE	26.58 ± 3.97	19.59 ± 1.73	0.74 ± 0.13	35.58 ± 5.90	42.14 ± 5.53	1.18 ± 0.25	70.87 ± 10.62	72.80 ± 8.97	1.03 ± 0.20
PG	681.31 ± 140.67	555.5 ± 74.68	0.82 ± 0.20	118.12 ± 15.64	144.08 ± 12.44	1.22 ± 0.19	89.73 ± 17.41	104.34 ± 18.95	1.16 ± 0.31
PI	296.99 ± 72.95	393.49 ± 54.45	**1.32 ± 0.37**	496.14 ± 76.05	592.65 ± 60.80	1.19 ± 0.22	590.29 ± 98.78	557.69 ± 114.42	0.94 ± 0.25
PS	505.23 ± 116.53	683.62 ± 85.94	**1.35 ± 0.36**	566.62 ± 68.42	717.63 ± 61.54	1.27 ± 0.19	247.79 ± 42.92	286.13 ± 46.89	1.15 ± 0.28
PA	509.27 ± 114.31	384.62 ± 59.29	0.76 ± 0.21	132.83 ± 23.68	161.84 ± 15.41	1.22 ± 0.25	68.18 ± 12.33	66.47 ± 12.02	0.97 ± 0.25
DG	4.40 ± 0.95	2.48 ± 0.33	**0.56 ± 0.14**	2.16 ± 0.49	1.80 ± 0.53	0.83 ± 0.31	14.64 ± 3.93	11.05 ± 1.83	0.75 ± 0.24
TG	501.88 ± 109.72	361.62 ± 38.47	0.72 ± 0.18	239.11 ± 36.13	256.90 ± 49.26	1.07 ± 0.26	826.26 ± 192.05	653.36 ± 152.10	0.79 ± 0.26
SM	313.55 ± 42.25	232.36 ± 28.24	0.74 ± 0.13	128.42 ± 20.99	165.52 ± 22	1.29 ± 0.27	468.76 ± 55.25	498.96 ± 75.61	1.06 ± 0.20
Cer	1.28 ± 0.37	0.88 ± 0.12	0.69 ± 0.22	1.12 ± 0.23	1.29 ± 0.25	1.16 ± 0.33	5.51 ± 1.23	5.67 ± 0.83	1.03 ± 0.27
MHC	0.63 ± 0.17	0.93 ± 0.13	**1.49 ± 0.46**	0.35 ± 0.08	0.55 ± 0.12	**1.56 ± 0.50**	1.08 ± 0.18	1.67 ± 0.28	**1.54 ± 0.37**
DHC	N.D.	N.D.	N.D.	0.13 ± 0.01	0.19 ± 0.04	**1.44± 0.36**	N.D.	N.D.	N.D.

[a]Underlined ratios have *P*-value < 0.05, and those in bold showed more than 30% change in their relative amounts.

320 lipid species in each tissue sample of WT and KO mice are listed in Table S1, represented with the relative peak area (vs IS) value of each lipid species and the relative change (KO/WT), along with *P*-values. Confirmed isomeric structures of PCs and PEs as well as possible isomeric TGs (without specifying the exact chain locations) are listed in Table S2.

Relative Changes in Total Lipids between WT and KO

Prior to a comprehensive comparison of individual lipid molecules in the different tissues of WT and KO mice, PCA was performed with the average peak area values of all 320 quantified species obtained from individual animals given in Table S1. The PCA plot in Figure 1 shows the overall differences in the global lipid profiles between WT and KO mice in lung, kidney, and liver tissues. The results show that lipids in the lung and liver exhibited clear differences in WT and p53 KO mice, whereas lipids in kidney showed similarity in WT and p53 KO mice. This can be visualized more clearly in the levels of different lipid classes by plotting the relative abundance of each lipid class of WT and p53 KO (Figure 2). Figure 2 compares each lipid category in lung, kidney, and liver tissues separately plotted as two parts (species detected in positive and negative ion modes of MS); the numbers in parentheses represent the normalized value in comparison with WT, which is set at 1.00, and the numbers belonging to each lipid class are the percentage values. While lipid classes detected in positive ion mode represented a 27% decrease in total amount (based on total relative peak area compared to that of IS) for KO lung tissue, the relative abundance of each individual lipid class (PC, TG, SM, PE, DG, Cer, and MHC) was almost unaffected (for instance, from 64.9% to 65% for PC). However, PA, PG, PI, and PS of lung tissue detected in negative ion mode (Figure 2A) exhibited no change in total amounts, but noticeable differences in the relative abundance of each lipid class were observed (for instance, from 24.5% to 33.9% for PS). In kidney tissue, the relative abundance of most lipid classes (PC, TG, SM, PS, PI, PA, and PG) was not changed but the total amounts of the PLs in both positive and negative ion mode increased by about 17−23%. Liver tissue exhibited some changes in relative abundances in most lipid classes (Figure 2C).

Lipid Classes with Significant Changes between WT and KO

While Figure 2 represents the change in overall amounts of each lipid class in WT and p53 KO mice organs, a direct comparison of the total amounts of each lipid class among different tissues is shown in Figure 3, providing a deeper understanding of the significance of variation in the specific lipid classes. Figure 3 shows a comparison of the relative amounts (summed values of relative peak area vs IS) of PI, PS, MHC, and TG from the three tissues, and bar graphs marked with asterisk (*) show a significant change (>30%, $P < 0.05$) in p53 KO tissue. Plots of the other eight lipid classes are given in Figure S1 of the Supporting Information, and data for all lipid classes are listed in Table 2. Data underlined in Table 2 represents a significant difference between KO and WT with *P*-value < 0.05, while underlined data in bold show greater than 30% change in amounts. In the case of lung tissue of p53 KO mice, the total levels of PC, PE, DG, and TG were significantly lowered by more than 30% but those of PI, PS, DG, and MHC were increased by about 30−50%. A recent study onthe lipid profiles of lung tissues from patients with nonsmall cell lung cancer (NSCLC)[32] reported similar results in which the overall amounts of PC and SM were decreased by about 20% and 48%, respectively, with cancer but showed an opposite trend for PS

DOI: 10.1021/acs.jproteome.6b00566
J. Proteome Res. 2016, 15, 3763−3772

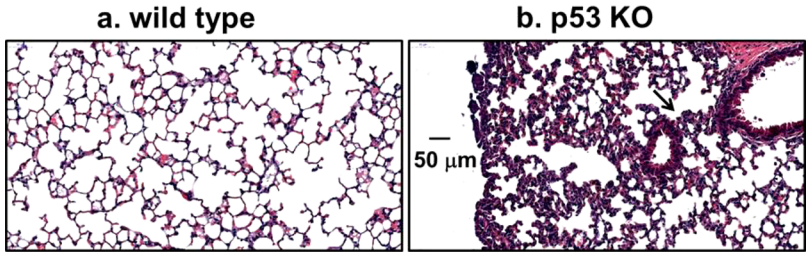

Figure 4. Micrographs of lung tissue in (A) WT mouse and (B) p53 KO mouse. Interstitial hyperplasia in alveolar lesion is distinct in p53 KO mouse (indicated by arrow).

(with 38% decrease). It is noteworthy that MHC was significantly increased by ~50% in all tissue types of p53 KO mice (Figure 3, although it had relatively low levels compared to other PLs. Similarly, DHC, which is present in relatively low levels, showed a 44% increase in kidney tissue only in p53 KO mice (Table 2). Table 2 also shows that there were distinct changes in levels in most lipid classes in the lung tissue, but significant changes were observed only in the MHC of all tissues and in DHC in the kidney tissue. Microscopic examination of stained tissues of the three organs showed that no significant changes under p53 deficiency were found in the kidney and liver. However, interstitial hyperplasia in alveolar was extensively observed in the lung tissue of a 5-month-old p53 KO mouse (Figure 4). Since interstitial hyperplasia in alveolar is a known preneoplastic change, histological changes in lung tissue can be affected, owing to the lack of p53 gene as compared to the other two organs.

Individual Lipid Molecules with Significant Changes between WT and KO

The influence of p53 knockout on the lipid profile of mice organs was further examined at the molecular levels, and a few lipid species showing significant changes (>30% and $P < 0.05$) in one of the three tissue types were selected for comparison (Table 3). The species shown in bold are the relatively abundant ones in each class (Table 3). p53 KO appears to influence some of the highly abundant lipid species in lung and liver tissues, whereas significant changes were observed in most of the relatively low levels of lipids. Highly abundant species in this study is defined as the species in which the percentage of abundance in each class is greater than $100/n$ (n: total number of lipid molecules in each class). Figure 5 shows the comparison of the relative ratio (KO/WT) of selected PC, PI, and PS species among the three tissue types, and Figure 6 shows the plots for DG and TG species. Lipid molecules marked in bold in Figure 5 are relatively abundant in each lipid class. A total of 43 PC molecules were quantified, and the results showed a significant decrease ($P < 0.05$) in PC levels (Table 2). However, a t-test of individual PC molecules showed that none of the PC species met the criteria (>30% change with $P < 0.05$). This discrepancy is possibly due to the fact that all 43 quantified PC species were decreased in our results and 13 highly abundant PC species, out of 43 quantified, exhibited about 20−50% decreases, but the results were not statistically significant (Table S1). For instance, highly abundant PC species such as 16:0-LPC (lysophosphatidylcholine), 18:0-LPC, 34:2-PC, and 36:2-PC showed about 20−30% decreases with KO; these species were reported to decrease in human plasma from patients with adenocarcinoma of the lung.[33] In addition, LPC (16:0, 18:0, 18:1, and 18:2) levels in plasma from patients with lung cancer were reported to decrease,[34] similar to the results in our study (Table S1). Although none of the lung PC species exhibited a change larger than 30% with $P < 0.05$, it is evident that the overall PC levels of lung tissue were significantly decreased with p53 KO. PC levels in kidney and liver tissues increased negligibly, but the increase was not significant. Instead, only 36:2-PC (18:0/18:2 and 18:1/18:1 in Table S-2a), highly abundant in the liver tissue of p53 deficient mice, was found to significantly increase by about 35%, as shown in Figure 5 and Table 3.

PI species with acyl chain structure of 16:0/22:6 showed a 35% increase in liver tissue, but most PI species shown in Figure 5 were increased in lung tissue after p53 KO. Among these, 18:0/20:4-PI was the most abundant (comprising about 53% of the relative amounts in PIs of WT lung tissue). This is similar to lipid profiles of lung tissues from patients with nonsmall cell lung cancer (NSCLC),[32] in which PI species (38:3, 40:3, and 38:2) were significantly increased although their chain structures were slightly different from our results. In kidney tissues of KO mice, 18:0/18:0-PI decreased by about 40% but 18:1/22:4-PI increased by 64% (Table 3). The decrease in 18:0/18:0-PI is in agreement with an earlier lipidomic study on human kidney tumor tissues.[35] In PS, six species showed significant changes in lung tissue and four of them (18:0/18:1, 18:0/22:5, 18:0/22:6, and 18:1/18:1) were found to be highly abundant, owing to increases of more than 40%. In addition, 16:0/18:0-PS (highly abundant in liver) was increased by about 50% in liver tissue. A report on lipid profiles from the plasma of patients with adenocarcinoma lung cancer showed that 36:1-PS (presumably 18:0/18:1) increased with the progression of cancer.[33] PIs and PSs containing a saturated acyl chain 18:0 were significantly increased in lung tissues (five out of six PIs and three PSs listed in Table 3) and in liver tissues (16:0/18:0-PS), except for 18:0/18:0-PI, which decreased in kidney tissues (Table 3). Similar results were also observed in PA species (Table 3): 18:1/18:0-PA and 18:0/20:0-PA in lung tissues and 18:0-LPA in kidney tissues.

Quantitative analysis of neutral GLs exhibits distinct differences in DG and TG levels, in which most individual species of DG and TG in both lung and liver tissues decreased (Table S1). The relative ratios of DG and TG species showing significant changes were plotted (Figure 6), and they revealed that (16:0,22:0)-DG decreased by 4-fold in liver and most TGs decreased by 50−70% in liver except 52:4-TG (which showed a 1.89-fold increase; Table 3). Only two TGs (56:0 and 56:6) were significantly decreased about 50% in liver. By examining the available molecular structures (Table S2c) in these 14 significantly decreased liver TG species, we found that they consisted of saturated acyl chains or monounsaturated acyl chain. A similar result was reported with the downregulation of 10 TGs in patients with cirrhosis and hepatocellular carcinoma

DOI: 10.1021/acs.jproteome.6b00566
J. Proteome Res. 2016, 15, 3763−3772

Table 3. Peak Area Ratio of Lipids Selected from Table S1 of the Supporting Information with Significant Changes (P-value < 0.05) in p53 KO Mice in Comparison with WT, for Lung, Kidney, and Liver Tissue Samples[a]

				Peak area				
Tissue	Class	Molecular species	m/z	WT	KO	KO/WT	Abun % (WT)	FDR corrected P-value
Lung	PI	18:0/18:1	863.6	1.95 ± 0.58	3.55 ± 0.44	1.82 ± 0.59	0.7	0.53
		18:0/18:2	861.6	4.58 ± 1.13	7.04 ± 0.79	1.54 ± 0.42	1.5	0.53
		18:0/20:4	**885.6**	**157.97 ± 41.68**	**215.98 ± 31.86**	**1.37 ± 0.41**	**53.2**	**0.53**
		18:0/20:5	883.6	1.23 ± 0.23	1.71 ± 0.20	1.39 ± 0.31	0.4	0.53
		18:0/22:4	913.6	1.67 ± 0.44	2.94 ± 0.40	1.77 ± 0.52	0.6	0.53
		20:0/20:4	913.6	0.08 ± 0.02	0.16 ± 0.03	1.89 ± 0.62	0.0	0.53
	PS	*16:1	494.3	0.16 ± 0.05	0.24 ± 0.04	1.54 ± 0.52	0.0	0.53
		18:0/18:1	**788.6**	**18.15 ± 3.23**	**30.37 ± 3.21**	**1.67 ± 0.35**	**3.6**	**0.53**
		18:0/22:5	**836.6**	**44.97 ± 12.43**	**69.12 ± 9.06**	**1.54 ± 0.47**	**8.9**	**0.53**
		18:0/22:6	**834.5**	**117.28 ± 23.29**	**175.47 ± 22.93**	**1.50 ± 0.36**	**23.2**	**0.53**
		18:1/18:1	**786.6**	**44.94 ± 11.41**	**63.67 ± 7.60**	**1.42 ± 0.40**	**8.9**	**0.53**
		22:6/20:4	854.6	0.34 ± 0.07	0.09 ± 0.01	0.27 ± 0.07	0.1	0.53
	PA	16:0	409.2	2.69 ± 0.86	3.60 ± 0.72	1.34 ± 0.50	0.5	0.53
		18:0/20:0	731.6	0.06 ± 0.02	0.15 ± 0.02	2.47 ± 1.01	0.0	0.53
		18:1/18:0	701.6	2.98 ± 0.60	5.57 ± 0.95	1.87 ± 0.49	0.6	0.53
	TG	56:0	936.8	0.04 ± 0.02	0.02 ± 0.00	0.43 ± 0.21	0.0	0.53
		56:6	924.9	0.32 ± 0.05	0.16 ± 0.03	0.51 ± 0.12	0.1	0.53
Kidney	PG	16:1	481.4	1.19 ± 0.15	1.66 ± 0.10	1.40 ± 0.19	1.0	0.78
		18:0	511.4	0.82 ± 0.11	1.15 ± 0.23	1.40 ± 0.33	0.7	0.46
		20:5/16:0	767.6	0.08 ± 0.02	0.12 ± 0.01	1.45 ± 0.30	0.1	0.44
	PI	18:0/18:0	865.6	1.26 ± 0.15	0.75 ± 0.08	0.59 ± 0.09	0.3	0.46
		18:1/22:4	911.6	0.09 ± 0.02	0.15 ± 0.02	1.64 ± 0.35	0.0	0.46
	PS	*16:1	494.3	0.09 ± 0.01	0.25 ± 0.06	2.68 ± 0.74	0.0	0.33
		18:0	524.3	6.65 ± 0.76	9.74 ± 2.22	1.47 ± 0.37	1.2	0.66
		20:5	542.3	0.03 ± 0.01	0.09 ± 0.02	2.87 ± 0.85	0.0	0.33
		18:0/20:1	816.6	0.14 ± 0.03	0.18 ± 0.03	1.34 ± 0.34	0.0	0.78
		18:0/20:5	808.6	4.83 ± 0.70	6.97 ± 0.72	1.44 ± 0.26	0.9	0.46
		18:0/22:2	842.7	0.37 ± 0.09	0.27 ± 0.03	0.72 ± 0.18	0.1	0.78
		18:0/22:3	840.6	0.24 ± 0.05	0.43 ± 0.06	1.78 ± 0.47	0.0	0.46
		18:0/22:4	838.6	0.99 ± 0.14	1.46 ± 0.16	1.48 ± 0.26	0.2	0.46
	PA	14:0	381.2	0.01 ± 0.00	0.01 ± 0.00	1.97 ± 0.64	0.0	0.66
		*18:0	437.2	1.42 ± 0.18	1.90 ± 0.28	1.33 ± 0.26	1.1	0.78
Liver	PC	**36:2**	**786.6**	**498.31 ± 43.58**	**673.13 ± 126.43**	**1.35 ± 0.28**	**17.0**	**0.55**
	PI	16:0/22:6	881.7	2.37 ± 0.59	3.21 ± 0.68	1.35 ± 0.44	0.4	0.55
	PS	**16:0/18:0**	**762.6**	**21.59 ± 4.84**	**32.39 ± 5.16**	**1.50 ± 0.41**	**8.7**	**0.55**
	PA	*18:0	437.2	1.31 ± 0.24	1.40 ± 0.23	1.07 ± 0.26	1.9	0.40
	DG	16:0,22:0	670.7	0.02 ± 0.00	0.00 ± 0.00	0.20 ± 0.06	0.1	0.24
	TG	42:0	740.7	0.08 ± 0.02	0.02 ± 0.00	0.25 ± 0.08	0.0	0.13
		42:1	738.7	0.02 ± 0.01	0.01 ± 0.00	0.50 ± 0.27	0.0	0.26
		44:0	768.8	0.58 ± 0.15	0.16 ± 0.04	0.28 ± 0.10	0.1	0.09
		44:1	766.8	0.49 ± 0.12	0.13 ± 0.04	0.27 ± 0.10	0.1	0.09
		44:2	764.8	0.21 ± 0.06	0.08 ± 0.02	0.38 ± 0.14	0.0	0.26
		46:0	796.8	1.06 ± 0.26	0.34 ± 0.09	0.32 ± 0.12	0.1	0.09
		46:1	794.8	3.31 ± 0.78	1.24 ± 0.28	0.37 ± 0.12	0.4	0.09
		46:2	792.8	1.53 ± 0.34	0.59 ± 0.13	0.39 ± 0.12	0.2	0.26
		48:1	**822.8**	**19.86 ± 4.41**	**8.70 ± 2.19**	**0.44 ± 0.15**	**2.4**	**0.09**
		48:2	820.8	9.60 ± 1.95	4.36 ± 0.84	0.45 ± 0.13	1.2	0.13
		48:3	818.8	4.11 ± 0.84	1.99 ± 0.39	0.48 ± 0.14	0.5	0.26
		50:0	852.8	9.41 ± 2.41	4.81 ± 1.28	0.51 ± 0.19	1.1	0.26
		52:4	**872.8**	**23.49 ± 5.15**	**44.48 ± 8.86**	**1.89 ± 0.56**	**2.8**	**0.55**
		54:0	908.8	1.54 ± 0.40	0.67 ± 0.14	0.44 ± 0.15	0.2	0.09
		54:1	906.8	9.39 ± 2.77	5.28 ± 1.66	0.56 ± 0.24	1.1	0.26

[a]Relative abundance is expressed with the peak area percentage (%) of each species within the corresponding lipid class. Species in bold are relatively abundant in each lipid group. (* species with significant changes found in other tissue types.)

(HCC) compared to healthy controls; however, the patterns of acyl chain structures in human TGs with significant decreases were different[36] from those observed in this study. Similar to the significant decrease in total TG levels of blood observed in patients with cirrhosis and HCC,[37,38] an abnormal decrease of TG level was seen in mice with p53 KO.

DOI: 10.1021/acs.jproteome.6b00566
J. Proteome Res. 2016, 15, 3763−3772

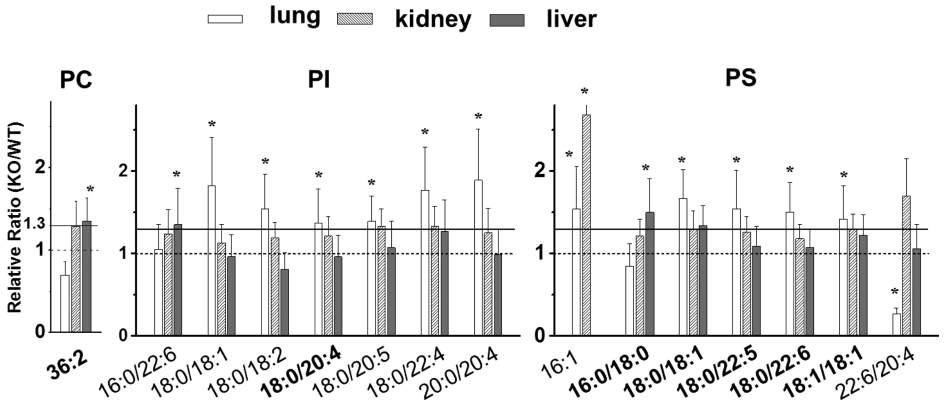

Figure 5. Relative changes (vs WT) of selected PC, PI, and PS species in p53 KO mice compared among three different tissue types. Types of tissue showing a significant change (>30%, $P < 0.05$) are marked with an asterisk (*). Species in bold represent a relatively abundant molecular type in each lipid category.

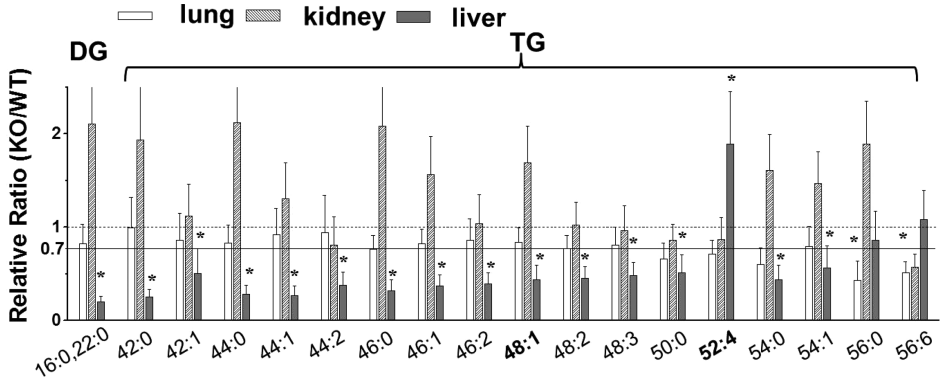

Figure 6. Relative changes (vs WT) of selected DG and TG species in p53 KO mice compared among three different tissue types. Types of tissue showing a significant change (>30%, $P < 0.05$) are marked with an asterisk (*). Species in bold represent a relatively abundant molecular type in each lipid category.

In order to enhance the declared significant data, the FDR corrected *P*-values were calculated and the threshold was set at 0.15 in this study. A total of 8 TGs out of 20 lipids from the liver tissue in Table 3 showed FDR corrected *P*-values less than 0.15, which strongly validates these species as statistically different between WT and KO. However, as the FDR corrected *P*-values were 0.53 for lipids from lung tissue and 0.33−0.78 for lipids from kidney tissue in Table 3, their alternations are not as significant as the aforementioned 8 hepatic TGs.

PCA was carried out with lipid species showing significant differences (>30%, $P < 0.05$) in WT and KO mice (Figure S2). Individual data points in the score plots represent individual animals (Figure S2), indicating that variations in lipid patterns among KO mice were greater than those in WT mice for all tissue types. This was further confirmed by the heat map of lipids among the three tissue types (Figure 7), showing the significant differences ($P < 0.05$) between the WT and p53 KO mice.

CONCLUSIONS

The influence of p53 KO on lipid profiles in mouse lung, kidney, and liver tissues was investigated by quantifying 320 lipid species (out of 399 identified species). Among the three tissues, lung tissue was the most significantly affected, owing to the lack of the p53 gene. Due to p53 KO, the total levels of PC, PE, DG, and TG decreased by about 30%, but those of PI, PS, DG, and MHC increased by 30−50%. It was found that

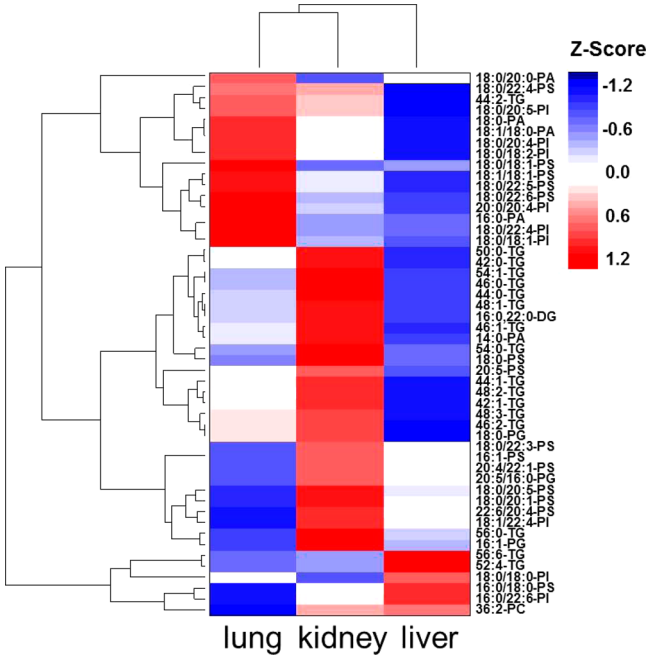

Figure 7. Heat map of lipids showing the differences among tissues between WT and p53 KO mice.

MHC levels increased in all tissues; however, the DHC level decreased only in kidney tissue. Variations in individual lipid

DOI: 10.1021/acs.jproteome.6b00566
J. Proteome Res. 2016, 15, 3763−3772

levels exhibited ubiquitous results in which most species of PIs, PSs, and PAs containing a saturated acyl chain (18:0) were significantly increased in both lung and liver tissue of p53 KO mice. Specifically, these changes were observed in relatively abundant species in each lipid class: 18:0/20:4-PI and 4 PSs (18:1/18:1, 18:0/22:6, 18:0/18:1, and 18:0/22:5) in lung tissue and 36:2-PC and 16:0/18:0-PS in liver tissue. Neutral GLs (16:0/22:0-DG and most TGs with saturated and monounsaturated acyl chains) decreased by 2−4-fold in liver tissue.

Although the mechanistic aspects relating p53 gene and cancer cells are not completely understood, it has been reported that mutated p53 gene is implicated in about 50% of cancers, such as stomach cancer and lung cancer.[39] We found that the molecular patterns of lipids, significantly altered by the lack of p53 in mouse, are slightly different from the molecular patterns of lipids in plasma or tissue samples of human carcinomas. However, the altered lipid profiles are tissue-specific. In humans, mutations or genetic alterations among patients with the same cancers can differ based on the tissue type and also based on primary or metastasized tumors. However, the present study has shown global lipidomic alterations among different tissues under the same genetic alteration—lack of p53 gene. This study provides a significant basis to understand the relationship between lipidomic changes and cancer development by systematically examining lipid profiles in the blood and urine from mice with a distinctive type of cancer.

■ ASSOCIATED CONTENT

Supporting Information

The Supporting Information is available free of charge on the ACS Publications website at DOI: 10.1021/acs.jproteome.6b00566.

Figure S1. Comparison of total peak area of 8 lipid categories (PC, PE, PG, PA, TG, SM, Cer, and DHC) from lung, kidney, and liver tissue between WT and p53 KO mice. Figure S2. Scores plots of principal component analysis (PCA) and loading plots based on lipids with significant differences ($P < 0.05$) in lung, kidney, and liver tissue between WT and p53 KO mice. Table S1. Peak area (relative to I.S.) values of each lipid species in lung, kidney, and liver tissue samples from WT and p53 KO mice and the relative ratio (KO/WT) with *P*-value. Species with bold represent the significant change (>30%, $P < 0.05$) in p53 KO mice. Peak area values with an underline represent that the corresponding lipid species in WT mice is relatively highly abundant in each lipid category. Numbers with asterisk (*) represent the lipid numbers identified with their molecular structures from CID spectra. Table S2. Isomeric acyl chains of (a) PC, (b) PE, and (c) TG species. The acyl chain locations of PC and PE were confirmed by CID spectra. For TG, the exact location of each acyl chain in a molecule is not differentiated. (PDF)

■ AUTHOR INFORMATION

Corresponding Authors

*E-mail: snumouse@snu.ac.kr. Phone: 82 2 880 1259. Fax: 82 2 873 1213.

*E-mail: mhmoon@yonsei.ac.kr. Phone: 82 2 2123 5634. Fax: 82 2 364 7050.

Notes

The authors declare no competing financial interest.

■ ACKNOWLEDGMENTS

This study was supported by a grant from the National Research Foundation of Korea (NRF-2015R1A2A1A01004677) and in part by a grant (NRF-2013M3A9B6046413) and a grant from the Bio & Medical Technology Development Program through the NRF funded by the Ministry of Science, ICT & Future Planning (Korea Mouse Phenotyping Center: 2013M3A9D5072550). This study was also partially supported by the Research Institute for Veterinary Science, Seoul National University and the Brain Korea 21 Program for Veterinary Science. The funders had no role in study design, data collection and analysis, decision to publish, or preparation of the manuscript.

■ ABBREVIATIONS

ACN, acetonitrile; Cer, ceramide; CID, collision-induced dissociation; CL, cardiolipin; DG, diacylglycerol; DHC, dihexosylceramide; ESI, electrospray ionization; FDR, false discovery rate; GalCer, galacrosylceramide; GluCer, glucosylceramide; IPA, isopropyl alcohol; KO, knockout; LacCer, lactosylceramide; LC, liquid chromatography; LPA, lysophosphatidic acid; LPC, lysophosphatidylcholine; LPE, lysophosphatidylethanolamine; LPG, lysophosphatidylglycerol; LPI, lysophosphatidylinositol; LPS, lysophosphatidylserine; MHC, monohexosylceramide; MS, mass spectrometry; MS/MS (or MS^2), tandem mass spectrometry; MTBE, methyl *tert*-butyl ether; *m/z*, mass-to-charge; PA, phosphatidic acid; PC, phosphatidylcholine; PCA, principal component analysis; PE, phosphatidylethanolamine; PG, phosphatidylglycerol; PI, phosphatidylinositol; PS, phosphatidylserine; SM, sphingomyelin; SRM, selected reaction monitoring; TG, triacylglycerol; UPLC, ultrahigh-performance liquid chromatography; WT, wild type

■ REFERENCES

(1) Siegel, R. L.; Miller, K. D.; Jemal, A. Cancer statistics, 2015. *Ca-Cancer J. Clin.* **2015**, *65*, 5−29.

(2) Greenblatt, M. S.; Bennett, W. P.; Hollstein, M.; Harris, C. C. Mutations in the p53 tumor suppressor gene: clues to cancer etiology and molecular pathogenesis. *Cancer Res.* **1994**, *54*, 4855−4878.

(3) Oren, M.; Rotter, V. Introduction: p53-the first twenty years. *Cell. Mol. Life Sci.* **1999**, *55*, 9−11.

(4) Vousden, K. H.; Lu, X. Live or let die: the cell's response to p53. *Nat. Rev. Cancer* **2002**, *2*, 594−604.

(5) Zhu, W. G.; Srinivasan, K.; Dai, Z.; Duan, W.; Druhan, L. J.; Ding, H.; Yee, L.; Villalona-Calero, M. A.; Plass, C.; Otterson, G. A. Methylation of adjacent CpG sites affects Sp1/Sp3 binding and activity in the p21(Cip1) promoter. *Mol. Cell. Biol.* **2003**, *23*, 4056−4065.

(6) Wang, X.; Zhao, X.; Gao, X.; Mei, Y.; Wu, M. A new role of p53 in regulating lipid metabolism. *J. Mol. Cell. Biol.* **2013**, *5*, 147−150.

(7) Zheng, J.; Lang, Y.; Zhang, Q.; Cui, D.; Sun, H.; Jiang, L.; Chen, Z.; Zhang, R.; Gao, Y.; Tian, W.; Wu, W.; Tang, J. Structure of human MDM2 complexed with RPL11 reveals the molecular basis of p53 activation. *Genes Dev.* **2015**, *29*, 1524−1534.

(8) Saldaña-Meyer, R.; González-Buendía, E.; Guerrero, G.; Narendra, V.; Bonasio, R.; Recillas-Targa, F.; Reinberg, D. CTCF regulates the human p53 gene through direct interaction with its natural antisense transcript, Wrap53. *Genes Dev.* **2014**, *28*, 723−734.

(9) Naguib, A.; Bencze, G.; Engle, D. D.; Chio, I. I.; Herzka, T.; Watrud, K.; Bencze, S.; Tuveson, D. A.; Pappin, D. J.; Trotman, L. C. P53 mutations change phosphatidylinositol acyl chain composition. *Cell Rep.* **2015**, *10*, 8−19.

(10) Glunde, K.; Ackerstaff, E.; Mori, N.; Jacobs, M. A.; Bhujwalla, Z. M. Choline phospholipid metabolism in cancer: consequences for molecular pharmaceutical interventions. *Mol. Pharmaceutics* **2006**, *3*, 496−506.

DOI: 10.1021/acs.jproteome.6b00566
J. Proteome Res. 2016, 15, 3763−3772

(11) Brouwers, J. F.; Vernooij, E. A.; Tielens, A. G.; van Golde, L. M. Rapid separation and identification of phosphatidylethanolamine molecular species. *J. Lipid Res.* **1999**, *40*, 164−169.
(12) Wright, M. M.; Howe, A. G.; Zaremberg, V. Cell membranes and apoptosis: role of cardiolipin, phosphatidylcholine, and anticancer lipid analogues. *Biochem. Cell Biol.* **2004**, *82*, 18−26.
(13) Taguchi, R.; Hayakawa, J.; Takeuchi, Y.; Ishida, M. Two-dimensional analysis of phospholipids by capillary liquid chromatography/electrospray ionization mass spectrometry. *J. Mass Spectrom.* **2000**, *35*, 953−966.
(14) Isaac, G.; Bylund, D.; Månsson, J. E.; Markides, K. E.; Bergquist, J. Analysis of phosphatidylcholine and sphingomyelin molecular species from brain extracts using capillary liquid chromatography electrospray ionization mass spectrometry. *J. Neurosci. Methods* **2003**, *128*, 111−119.
(15) Hu, C.; Van Dommelen, J.; Van Der Heijden, R.; Spijksma, G.; Reijmers, T. H.; Wang, M.; Slee, E.; Lu, X.; Xu, G.; Van Der Greef, J.; Hankemeier, T. RPLC−Ion−Trap−FTMS method for lipid profiling of plasma: Method validation and application to p53 mutant mouse model. *J. Proteome Res.* **2008**, *7*, 4982−4991.
(16) Zhao, Z.; Xiao, Y.; Elson, P.; Tan, H.; Plummer, S. J.; Berk, M.; Aung, P. P.; Lavery, I. C.; Achkar, J. P.; Li, L.; Casey, G.; Xu, Y. Plasma lysophosphatidylcholine levels: potential biomarkers for colorectal cancer. *J. Clin. Oncol.* **2007**, *25*, 2696−2701.
(17) Kim, H.; Min, H. K.; Kong, G.; Moon, M. H. Quantitative analysis of phosphatidylcholines and phosphatidylethanolamines in urine of patients with breast cancer by nanoflow liquid chromatography/tandem mass spectrometry. *Anal. Bioanal. Chem.* **2009**, *393*, 1649−1656.
(18) Kim, H.; Min, H. K.; Kong, G.; Moon, M. H. Quantitative analysis of urinary phospholipids with breast cancer by nanoflow liquid chromatography−tandem mass spectrometry: II. Negative ion mode analysis of four phospholipid classes. *Anal. Bioanal. Chem.* **2010**, *396*, 1273−1280.
(19) Meshkani, R.; Adeli, K. Hepatic insulin resistance, metabolic syndrome and cardiovascular disease. *Clin. Biochem.* **2009**, *42*, 1331−1346.
(20) Min, H. K.; Lim, S.; Chung, B. C.; Moon, M. H. Shotgun lipidomics for candidate biomarkers of urinary phospholipids in prostate cancer. *Anal. Bioanal. Chem.* **2011**, *399*, 823−830.
(21) Lim, S.; Bang, D. Y.; Rha, K. H.; Moon, M. H. Rapid screening of phospholipid biomarker candidates from prostate cancer urine samples by multiple reaction monitoring of UPLC-ESI-MS/MS and statistical approaches. *Bull. Korean Chem. Soc.* **2014**, *35*, 1133−1138.
(22) Byeon, S. K.; Lee, J. Y.; Lee, J. S.; Moon, M. H. Lipidomic Profiling of Plasma and Urine from Patients with Gaucher Disease During Enzyme Replacement Therapy by Nanoflow Liquid Chromatography−Tandem Mass Spectrometry. *J. Chromatogr. A* **2015**, *1381*, 132−139.
(23) Bang, D. Y.; Moon, M. H. On-line Two−dimensional Capillary Strong Anion exchange /Reversed Phase Liquid Chromatography−Tandem Mass Spectrometry for Comprehensive Lipid Analysis. *J. Chromatogr. A* **2013**, *1310*, 82−90.
(24) Moon, M. H. Phospholipid analysis by nanoflow liquid chromatography−tandem mass spectrometry. *Mass Spectrom. Lett.* **2014**, *5*, 1−11.
(25) Wymann, M. P.; Schneiter, R. Lipid signalling in disease. *Nat. Rev. Mol. Cell Biol.* **2008**, *9*, 162−176.
(26) Santos, C. R.; Schulze, A. Lipid metabolism in cancer. *FEBS J.* **2012**, *279*, 2610−2623.
(27) Eberlin, L. S.; Gabay, M.; Fan, A. C.; Gouw, A. M.; Tibshirani, R. J.; Felsher, D. W.; Zare, R. N. Alteration of the lipid profile in lymphomas induced by MYC overexpression. *Proc. Natl. Acad. Sci. U. S. A.* **2014**, *111*, 10450−10455.
(28) Byeon, S. K.; Lee, J. Y.; Moon, M. H. Optimized Extraction of Phospholipids and Lysophospholipids for Nanoflow Liquid Chromatography−Electrospray Ionization-Tandem Mass Spectrometry. *Analyst* **2012**, *137*, 451−458.
(29) Lim, S.; Byeon, S. K.; Lee, J. Y.; Moon, M. H. Computational Approach to the Structural Identification of Phospholipids Using Raw Mass Spectra from Nanoflow Liquid Chromatography−Electrospray Ionization-Tandem Mass Spectrometry. *J. Mass Spectrom.* **2012**, *47*, 1004−1014.
(30) Ahn, E.; Kim, H.; Chung, B. C.; Moon, M. H. Quantitative Analysis of Phosphatidylcholine in Rat Liver Tissue by Nanoflow Liquid Chromatography/Tandem Mass Spectrometry. *J. Sep. Sci.* **2007**, *30*, 2598−2604.
(31) Bang, D. Y.; Lim, S.; Moon, M. H. Effect of Ionization Modifiers on the Simultaneous Analysis of All Classes of Phospholipids by Nanoflow Liquid Chromatography/Tandem Mass Spectrometry in Negative Ion Mode. *J. Chromatogr. A* **2012**, *1240*, 69−76.
(32) Marien, E.; Meister, M.; Muley, T.; Fieuws, S.; Bordel, S.; Derua, R.; Spraggins, J.; Van de Plas, R.; Dehairs, J.; Wouters, J.; Bagadi, M.; Dienemann, H.; Thomas, M.; Schnabel, P. A.; Caprioli, R. M.; Waelkens, E.; Swinnen, J. V. Non−small cell lung cancer is characterized by dramatic changes in phospholipid profiles. *Int. J. Cancer* **2015**, *137*, 1539−1548.
(33) Ravipati, S.; Baldwin, D. R.; Barr, H. L.; Fogarty, A. W.; Barrett, D. A. Plasma lipid biomarker signatures in squamous carcinoma and adenocarcinoma lung cancer patients. *Metabolomics* **2015**, *11*, 1600−1611.
(34) Dong, J.; Cai, X.; Zhao, L.; Xue, X.; Zou, L.; Zhang, X.; Liang, X. Lysophosphatidylcholine profiling of plasma: discrimination of isomers and discovery of lung cancer biomarkers. *Metabolomics* **2010**, *6*, 478−488.
(35) Cífková, E.; Holčapek, M.; Lísa, M.; Vrána, D.; Melichar, B.; Študent, V. Lipidomic differentiation between human kidney tumors and surrounding normal tissues using HILIC−HPLC/ESI−MS and multivariate data analysis. *J. Chromatogr. B: Anal. Technol. Biomed. Life Sci.* **2015**, *1000*, 14−21.
(36) Chen, S.; Peiyuan, Y.; Zhao, X.; Xing, W.; Hu, C.; Zhou, L.; Xu, G. Serum lipid profiling of patients with chronic hepatitis B, cirrhosis, and hepatocellular carcinoma by ultra fast LC/IT−TOF MS. *Electrophoresis* **2013**, *34*, 2848−2856.
(37) Tietge, U. J.; Boker, K. H.; Bahr, M. J.; Weinberg, S.; Pichlmayr, R.; Schmidt, H. H.; Manns, M. P. Lipid parameters predicting liver function in patients with cirrhosis and after liver transplantation. *Hepato-gastroenterol.* **1997**, *45*, 2255−2260.
(38) Jiang, J.; Zhang, X.; Wu, C.; Qin, X.; Luo, G.; Deng, H.; Lu, M.; Xu, B.; Li, M.; Ji, M.; Xu, N. Increased plasma apoM levels in the patients suffered from hepatocellular carcinoma and other chronic liver diseases. *Lipids Health Dis.* **2008**, *7*, 1−5.
(39) Slee, E. A.; O'Connor, D. J.; Lu, X. To die or not to die: how does p53 decide? *Oncogene* **2004**, *23*, 2809−2818.

DOI: 10.1021/acs.jproteome.6b00566
J. Proteome Res. 2016, 15, 3763−3772